Phenothiazine-Based Self-Assembled Monolayer with Thiophene Head Groups Minimizes Buried Interface Losses in Tin Perovskite Solar Cells

Valerio Stacchini[§ 1,3], Madineh Rastgoo[§ 2], Mantas Marčinskas[5], Chiara Frasca[1,3], Kazuki Morita[1], Lennart Frohloff[4], Antonella Treglia[6], Orestis Karalis[1], Vytautas Getautis[5], Annamaria Petrozza[6], Norbert Koch[1,4], Hannes Hempel[1], Tadas Malinauskas[5*] ,Antonio Abate[1,2,3*], Artem Musiienko[1,7*]

1. Helmholtz-Zentrum Berlin für Materialien und Energie GmbH, 12489 Berlin, Germany

2. Department of Chemical, Materials and Production Engineering, University of Naples Federico II, Fuorigrotta, Italy

3. Department of Chemistry, University of Bielefeld, Universitätsstraße 25, 33615 Bielefeld, Germany

4. Institut für Physik & Center for the Science of Materials (CSMB), Humboldt-Universität zu Berlin, 12489, Berlin

5. Department of Organic Chemistry, Kaunas University of Technology, Radvilenu pl. 19, Kaunas LT-50254, Lithuania

6. Istituto Italiano di Tecnologia (IIT), via Rubattino 81, 20134, Milan, Italy

7. Humboldt-Universität zu Berlin, Zum Großen Windkanal 2, 12489 Berlin, Germany

§ These authors contributed equally to this work

* Corresponding authors: artem.musiienko@helmholtz-berlin.de, antonio.abate@helmholtz-berlin.de, tadas.malinauskas@ktu.lt

Keywords: Self-assembled Monolayers, Buried Interface, Phenothiazine, Tin perovskite, Solar Cells, DMSO-free, Lead-free

Abstract

Self-assembled monolayers (SAMs) have revolutionized the fabrication of lead-based perovskite solar cells, but they remain underexplored in tin perovskite systems. PEDOT is the material of choice for hole-selective layers in tin perovskite solar cells (TPSCs), but presents challenges for both performance and stability. MeO-2PACz, the only SAM reported for Sn perovskites, enables device fabrication but consistently underperforms when compared to PEDOT. In this work, we identify that MeO-2PACz's limitations arise from excessively strong interactions with perovskite surface and poor lattice matching, leading to poor interface quality. To overcome these issues, we design, synthesize, and characterize a novel SAM-forming molecule called Th-2EPT. Th-2EPT optimizes coordination strength and improves lattice compatibility, contributing to the creation of a high-quality buried interface and dramatically suppressing non-radiative recombination. We used Density Functional Theory (DFT) to evaluate coordination strength and lattice compatibility, complemented by nanosecond-resolution optical characterization techniques to confirm significantly reduced interfacial recombination and enhanced carrier lifetimes in Th-2EPT/Perovskite films. With Th-2EPT, we demonstrated the first SAM-based tin perovskite solar cells to outperform PEDOT-based devices, delivering a record power conversion efficiency (PCE) of 8.2% with a DMSO-free solvent system.

Introduction

Thanks to their simple processing, bandgap tunability, and defect tolerance, perovskites are on track to radically change the world of photovoltaics. However, two significant issues must be addressed before this technology can be considered competitive for commercialization: long-term stability and lead toxicity[1–4]. Intense research is focused on developing non-toxic alternatives to mitigate the toxicity issues of lead-containing perovskites[2,5,6]. Tin perovskite solar cells are potentially even more stable than their lead-based counterparts, exhibiting negligible ion migration[3,7,8]. Despite their potential, TPSCs underperform compared to their lead counterparts, hindered by rapid crystallizationdefective thin films[2] due to the facile oxidation of Sn^{2+} to Sn^{4+}, and poor energy-level alignment between standard selective contacts and the absorber layer[1,2,8–10]. Until now, in most studies on tin perovskite solar cells, poly(3,4-ethylene dioxythiophene) polystyrene sulfonate, in short PEDOT:PSS, has been the hole-selective layer (HSL) of choice, despite the significant energetic misalignment, acidity, and hygroscopicity that limit the performance of PEDOT-based devices and lead to device degradation[2,11–14]. Self-assembled monolayers (SAMs) present a promising alternative to PEDOT due to their dual role in interface passivation and charge selectivity[15–17]. While SAMs have demonstrated success in lead-based perovskites by improving charge extraction and passivating interfaces, their application in tin perovskites remains underexplored. To the best of our knowledge, MeO-2PACz is the only SAM successfully employed for tin perovskites, achieving moderate power conversion efficiencies (PCEs) of 5.8%[9] and 9.4%[18], achieved with a DMSO-free and DMSO solvent system, respectively. In any case, SAM-based solar cells have yet to outperform PEDOT controls, and the underlying causes of poor performance remain unclear[2,18–20]. In this work, we employ a DMSO-free solvent system for tin PSCs to mitigate solvent-induced degradation, addressing two key challenges: the oxidation of Sn^{2+} by DMSO and the presence of residual DMSO, which can further promote oxidation over the device's lifetime. Furthermore, we use first-principles calculations to identify the limitations of MeO-2PACz, revealing its strong interaction with the $FASnI_3$ lattice and dimensional mismatch as the cause for a highly defective interface. To overcome this incomaptibility between the MeO-2PACz and tin perovskite, we design and synthesize a novel SAM molecule, {2-[3,7-di(thiophen-3-yl)-10H-phenothiazin-10-yl]ethyl}phosphonic acid or Th-2EPT, featuring two thiophene passivating head groups, a phenothiazine core and a phosphonic acid anchoring group. Th-2EPT significantly improved the interfacial quality of tin perovskites by enhancing lattice matching and fine-tuning interaction strength. Ultra-fast time-resolved photoluminescence and transient absorption spectroscopy revealed significantly longer carrier lifetimes and reduced defect density for Th-2EPT, demonstrating its ability to suppress trap states and passivate the buried interface. Leveraging these improved optoelectronic properties, devices with Th-2EPT achieved a record power

conversion efficiency (PCE) of 8.2% with a DMSO-free solvent system and $EDA_{0.05}FA_{0.95}SnI_3$ as absorbing layer. This work marks the first successful attempt to fabricate a SAM-based DMSO-free tin perovskite solar cell that outperforms PEDOT.

Results and Discussion

In Pb-based perovskite solar cells, MeO-2PACz is commonly employed as one of the most efficient hole-selective materials available[17,21,22]. On the other hand, the effects of SAM passivation on Sn-based perovskite have never been studied in detail, and the underperformance of MeO-2PACz for this material remains a puzzling challenge[9,18,23]. This observation led us to hypothesize that a problematic interaction between MeO-2PACz and tin perovskite might be the source of this underperformance. We investigated whether MeO-2PACz could be incompatible with the lattice, thereby inducing a distorted and defective buried interface.[17,24,25]. We further postulated that the key to improving interfacial quality and suppressing interfacial recombination is not maximizing interaction strength, but rather achieving an optimal level, strong enough to passivate intrinsic interfacial defects, yet not too strong to interfere with perovskite growth[17,25]. In addition to interaction strength, we identified lattice matching as a critical factor. Poor lattice matching between the substrate and growing perovskite can result in structural defects and significant lattice strain at the interface[24,26]. An even worse scenario arises when a poor lattice match is coupled with a strong SAM-perovskite interaction. In this case, the two factors can amplify negatively, leading to a strained and defective interface. To investigate this further, we employed density functional theory (DFT) calculations to analyze lattice matching and binding energy of MeO-2PACz with the $FASnI_3$ perovskite lattice. Afterward, we performed the same calculations on a newly synthesized phenothiazine-based SAM molecule called Th-2EPT. In this section, we compare MeO-2PACz and Th-2EPT, simultaneously evaluating interaction strength and lattice matching with Sn perovskite and the interplay of these factors. As shown in Figure 1a, both molecules present two functional head groups, methoxy groups for MeO-2PACz and thiophenes in Th-2EPT. Both groups can behave as Lewis bases and interact with an undercoordinated Sn^{2+} ion in perovskite[27–30]. In this case, the Sn^{2+} ion acts as the Lewis acid in forming a Lewis acid-base adduct[25,31]. A graphical representation of this interaction is provided in Figure 1b. Due to the highly electronegative oxygen atom, the methoxy groups present a localized electron density and bind strongly with Sn^{2+}. Thiophenes instead bind more weakly because of the less ionic bonding environment and sulfur's lower electronegativity. To extract a quantitative value for the bond strength, the two molecules were modeled on a SnI_2-terminated surface of $FASnI_3$ perovskite, calculating the binding energy of the molecules through their head groups. Figure 1f shows the molecules' interaction on the $FASnI_3$ lattice with the DFT-calculated binding energies for both SAMs. MeO-2PACz exhibits a higher binding energy of 0.45 eV, attributed to the strong, polar nature of the O-Sn coordination. In contrast, Th-2EPT shows a weaker binding energy of 0.14
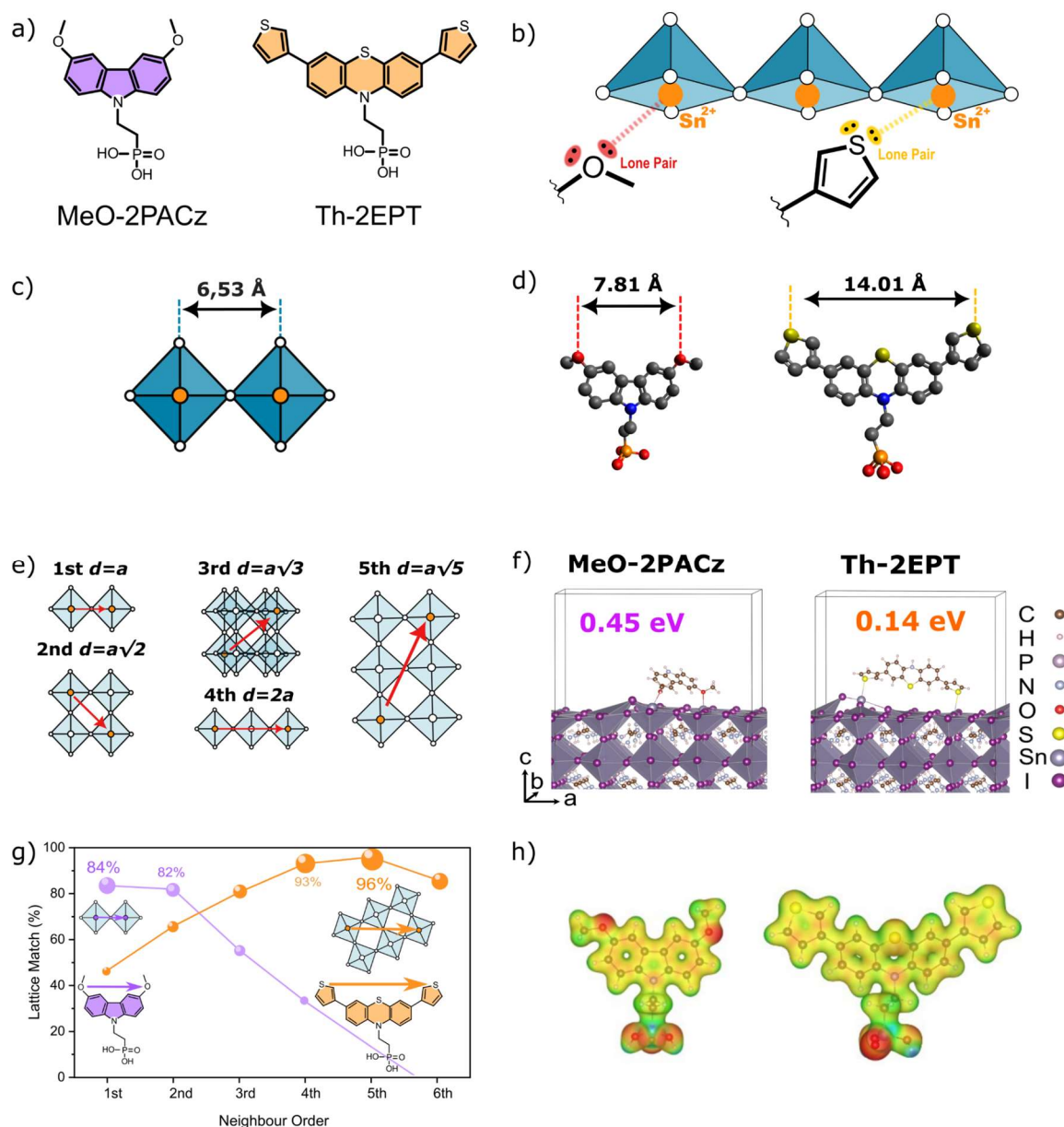
Figure 1: **(a)** Molecular structures of MeO-2PACz and Th-2EPT. **(b)** Mode of interaction between a FASnI₃ perovskite interface and SAMs head groups. Lewis adducts are formed between undercoordinated Sn ions in perovskite and the SAMs' head groups. **(c)** FASnI₃ lattice parameter, which is always equal to the Sn-Sn distance in the cubic lattice. **(d)** Distance between head groups, namely methoxy groups in MeO-2PACz and thiophene groups in Th-2EPT. **(e)** Distances of nearest neighboring Sn^{2+} in FASnI₃ and relative lattice vector. **(f)** DFT-calculated binding energies for the two molecules on top of a SnI2-terminated FASnI₃ surface. To focus on the head groups interaction, the calculation was performed on molecules without the phosphonic acid anchoring groups. **(g)** Geometric lattice matching for SAMs in their most favorable configurations: MeO-2PACz aligns best with the first and second nearest neighbors, while Th-2EPT aligns with the fourth and fifth neighbors. Overall, Th-2EPT exhibits superior alignment. **(h)** Electrostatic potential maps showing strong negativity (red) around the MeO oxygen atoms in MeO-2PACz and suppressed negativity (yellow) around the sulfur atoms in Th-2EPT.

eV, reflecting the lower electronegativity of sulfur and the slightly less polarized interaction with Sn^{2+}. Our calculations confirmed the hypothesis that MeO-2PACz forms strong bonds with Sn^{2+}, but its poor lattice compatibility compromises its effectiveness. This results in a weaker binding with Sn^{2+}, potentially allowing for more bond flexibility. To complement the binding energy analysis, the geometric compatibility and lattice matching of the terminal head groups of the SAMs with the perovskite lattice are evaluated. The geometric analysis of lattice matching is based on the hypothesis that SAMs interact with perovskite by forming Lewis adducts between the SAM's head groups (methoxy or thiophene) and undercoordinated Sn^{2+}. Head groups are two in each molecule, so the case where both bind to an Sn^{2+} ion is the most favorable. In this scenario, the possibility that the distance of the head groups between each other coincides with two neighboring Sn^{2+} ions is evaluated. For this reason, every combination of the nearest Sn-Sn couple in the perovskite lattice is assessed and compared with the characteristic distances of head groups in the SAM molecules. In the perovskite lattice, the distance to the n-th neighbor is given by the formula $d = a\sqrt{n_x^2 + n_y^2 + n_z^2}$, where a is the cubic lattice parameter, and n_x, n_y, n_z are the relative directional vectors. The characteristic dimensions of the perovskite lattice and the molecules are shown in Figure 1c and Figure 1d, while the distance of 1st to 5th nearest neighboring Sn^{2+} ions is shown in Figure 1e. The plot in Figure 1g displays the lattice matching percentage of the two SAMs with the nearest neighboring Sn^{2+} ions in the $FASnI_3$ cubic lattice. From the plot, the superior geometric compatibility of Th-2EPT with the perovskite lattice is evident. The S-S distance in Th-2EPT (~14.01 Å) aligns closely with the fifth nearest Sn-Sn neighbors in the $FASnI_3$ lattice ($d = a\sqrt{5}$ = 14.6 Å), achieving an almost perfect lattice match with 96% compatibility. In comparison, the O-O distance in MeO-2PACz (~7.81 Å) best aligns only with the second nearest neighbors (~9.22 Å), resulting in an 85% lattice match. It is important to note that the calculation considered the nearest neighboring ions in all directions for a cubic 3D lattice, so this consideration is very general and independent of lattice orientations. In this section, we have determined through theoretical considerations and calculations that, while MeO-2PACz forms stronger bonds, it shows an inferior lattice match with $FASnI_3$ perovskite. Conversely, Th-2EPT achieves superior lattice matching and a weaker but more flexible bonding. We postulate that this combination of factors might be decisive for forming a high-quality interface. In the following sections, measurements on films and solar cells are performed to support this hypothesis further.

Optical characterization

To assess the quality of the interface and further investigate the differences induced by different substrates, we initially analyzed the dependence of Voc with light intensity to extract the ideality factor. We conducted static and time-resolved photoluminescence, as well as photoluminescence quantum yield (PLQY) at different excitation densities and optical transient absorption spectroscopy (TAS), on perovskite films deposited on glass and on perovskite grown on the selective layers. PEDOT was included as a reference in this stage of the study, given its role as the most well-known hole selective layer (HSL) in FASnI$_3$ solar cells[9,20]. First, Voc dependence on light intensity was measured to extract the ideality factor, which quantifies deviation from ideal diode behavior and it is a useful index of non-radiative recombination at the interface. While an ideal cell has n=1, tin perovskite solar cells can show high ideality factors due to intense bulk and interfacial recombination. By measuring Voc across varying light intensities, the ideality factor was extracted using an equation easily derived from the diode equation in open circuit conditions: $n = \frac{q}{kT} \frac{\partial Voc}{\partial I}$. The extracted values for n resulted in 2.86, 2.18, and 1.98 for MeO-2PACz, PEDOT, and Th-2EPT, respectively (Figure 2d). The lower ideality factor with Th-2EPT is an indicator of reduced non-radiative recombination as it is closer to ideality. Then, photoluminescence decay were measured on half stacks of ITO/HSL/Perovskite, to investigate mainly the HTL/Perovskite interface. PL transients show a clear difference in decay times between the extraction layers, with Th-2EPT showing the slowest decay (Figure 2b). trPL data was then fitted with a bi-exponential decay model (fitting parameters and plots provided in Figure S4 of the supporting material) and the fit was used to the compute differential lifetimes $t = -\{d \ln[f_{(t)}]/dt\}^{-1}$, where $f_{(t)}$ is the time-dependent photon flux. In this model, the plateau visible for all curves after the first rise represents a visualization of the carrier lifetime[32,33] (Figure 2c). Reaching the plateau at only 33 ns, PEDOT records the shortest lifetime, followed by MeO-2PACz, which exhibits a lifetime of 63 ns, while the film on Th-2EPT achieves a longer lifetime of 93 ns. The perovskite grown on quartz exhibits a lifetime of 156 ns - an impressive value for tin perovskites - thereby confirming the exceptional quality of the thin films synthesized in this study. Following trPL, Transient absorption spectroscopy (TAS) was performed to further study recombination mechanisms in the films. TAS measures the relative change in transmittance of the material (photobleach) as function of time after the material is photoexcited. The resulting signal is proportional to the population of holes and electrons in the VB and CB, respectively. This enables tracking not only radiative recombination (as observed in time-resolved photoluminescence), but also carriers that follow non-radiative pathways. With a temporal resolution of about 300 fs TAS allows to study excited states and their recombination dynamics up to microseconds. For this measurement,

the samples were illuminated from the HTL side and a 343 nm laser was employed to obtain an excitation profile predominantly localized at the interface, due to the low penetration depth of low wavelengths in perovskite. In Figure 2e, the carrier dynamics are extracted at the photobleach maximum (around 850 nm - full spectra available in the supporting material in Figure S2) . A similar trend to trPL is observed, with perovskite on PEDOT showing fastest decay and the SAMs MeO-2PACz and Th-2EPT achieving longer lifetimes, close to the perovskite grown on glass. Notably, a trapped carrier contributes indirectly to the TAS signal by leaving an unbalanced charge in the other band. This produces a long-lived signal (in the microseconds time-range) that is proportional to the density of trapped carriers[34]. Indeed, in the microseconds range, the TAS signal decays quickly for Th-2EPT, while such signal is enhanced in the case of MeO-2PACz [34]. This result further supports the beneficial role of Th-2EPT in defect passivation and interaction with perovskite while it also strengthens the hypothesis of the he PL quantum yield (PLQY) as a function of excitation density, shown in Figure 2f, reveals an improvement in radiative efficiency at low excitation densities for perovskite films deposited on MeO-2PACz and Th-2EPT. This suggests effective interface passivation, in contrast to PEDOT, where the radiative efficiency is consistently reduced across all excitation densities, as evidenced by the normalized data in Figure SI 12b.
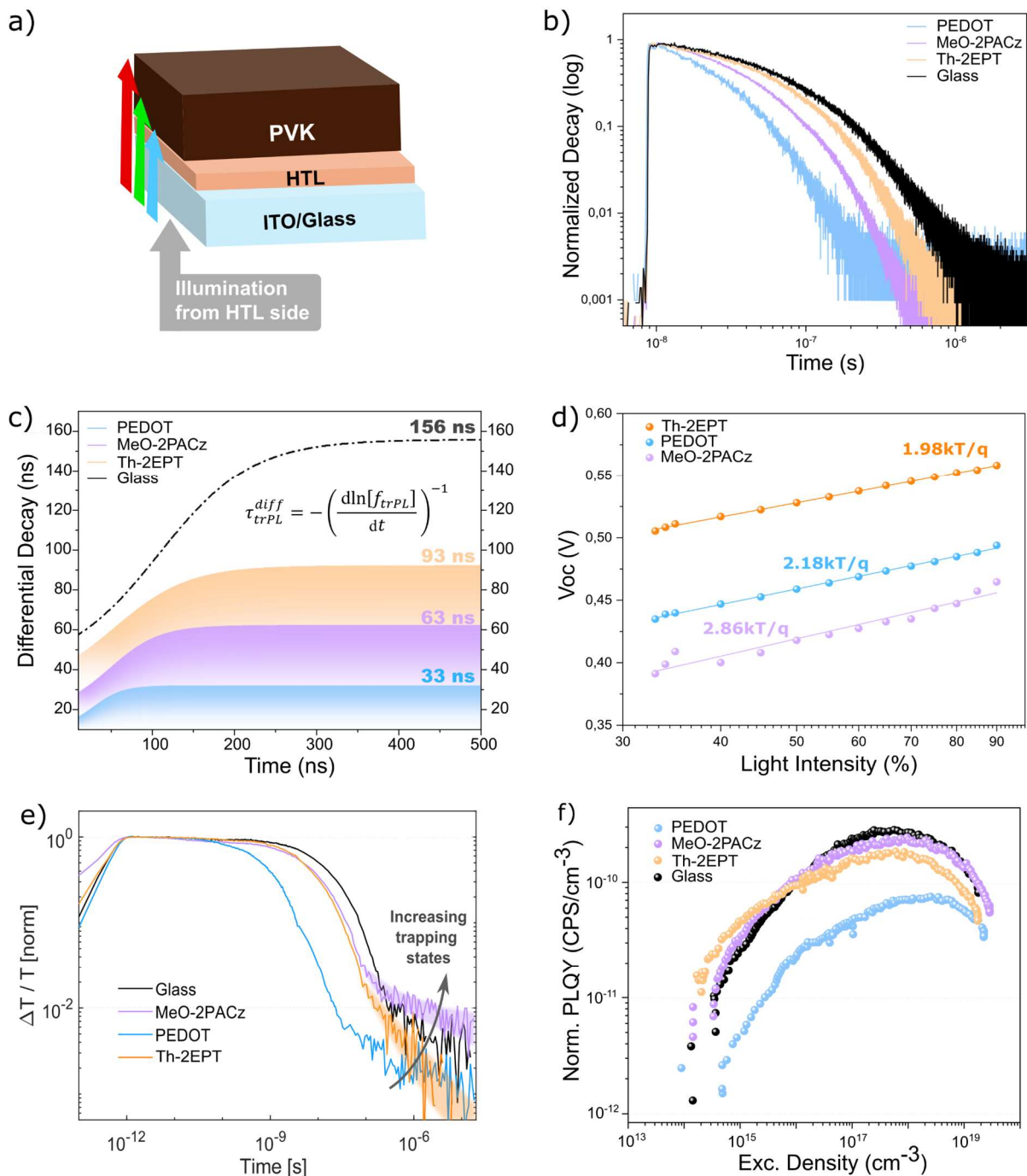
Figure 2 (a) Schematic representation of the ITO/HTL/PVK stack on which the measurements were performed. The colored arrows qualitatively represent the penetration depth dependance on excitation wavelength. **(b)** Normalized photoluminescence transients (trPL) displayed in logarithmic time and **(c)** computed differential lifetimes from double exponential fits to the trPL transients. **(d)** Open circuit voltage dependence on light intensity for solar cell devices . **(e)** Transient absorption (TAS) decays showing the decay of the photo bleach peak at 850 nm, with excitation density of $4 \cdot 10^{17}$ cm^{-3}. Full TAS spectra are available in the supporting information, Figure S2. **(f)** PLQY plots obtained by integrating the PL spectrum as function of excitation density.

Solar Cell Fabrication

To validate the theoretical predictions and assess the real impact of the SAMs on device performance, we fabricated solar cells incorporating MeO-2PACz, PEDOT, and Th-2EPT as hole-selective layers and tin perovskite $EDA_{0.05}FA_{0.95}SnI_3$ as the absorber.. Our approach avoids the use of DMSO, which despite being the most commonly used solvent for preparing tin perovskite, has also being identified as one of the sources of the Sn^{2+} oxidation[31,35]. Instead, we employed a solvent system composing of a mixture of DEF (N,N'-Diethylformamide) and DMPU (N,N′-Dimethylpropyleneurea) Among the candidates, the phenothiazine-based Th-2EPT demonstrated superior performance, achieving a record efficiency of 8.2% and surpassing MeO-2PACz (4.5%) and PEDOT (7.1%).The device architecture consists of ITO/HSL/DMSO-free Sn Perovskite/C60/BCP/Ag, where the HSL was varied between the three materials. Spin-coating and dip-coating were evaluated for Th-2EPT, with superior results obtained via dip-coating. The solar cell performance is summarized in Figure 3, which shows champion J-V curves (Figure 3b), EQE spectra (Figure 3c), Voc boxplots (Figure 3d), and PCE boxplots (Figure 3e). Th-2EPT demonstrated improved short-circuit current density (Jsc), delivering 18.8 mA/cm² compared to MeO-2PACz (14.9 mA/cm²) and PEDOT (18.4 mA/cm²). Incident photon current efficiency (IPCE) measurements were performed on champion pixels from the J-V plots (Figure 3b) to investigate this improvement. The IPCE spectrum confirmed the high Jsc of Th-2EPT devices, with a value of 18.97 mA cm^{-2}, compared to 14.99 mA cm^{-2} for MeO-2PACz and 17.67 mA cm^{-2} for PEDOT (Figure 3c). The EQE spectrum highlights the superior quantum efficiency of Th-2EPT, particularly at shorter wavelengths (Figure 3c), with an exceptionally high internal photon-to-electron conversion at 400 nm, far exceeding PEDOT and MeO-2PACz devices. Short wavelengths in the range 350-450 nm have low penetration depth in perovskite and are readily absorbed in the first nanometers, in the proximity of the HTL/Perovskite interface. For this reason, a substantial IPCE improvement at low wavelengths suggests improved interface quality and reduced non-radiative recombination at the Th-2EPT interface[36]. Open circuit voltage (Voc) is also significantly enhanced in Th-2EPT devices compared to PEDOT and MeO-2PACz. Champion Voc values of 0.63 V, 0.57 V, and 0.50 V were recorded for Th-2EPT, PEDOT, and MeO-2PACz, respectively (Figure 1d). Overall, Th-2EPT champion devices outperform PEDOT and MeO-2PACz in all solar cell parameters. Fill factor and short circuit current boxplots are shown in Figure S4 of the supporting information. These findings highlight the superior passivation properties of Th-2EPT, demonstrating its potential to significantly enhance the performance and efficiency of tin perovskite solar cells compared to conventional hole-selective layers. With 8.2% PCE ourTh-2EPT champion device is a record to the best of our knowledge for SAM-based, DMSO-free tin perovskite solar cells. Moreover, this PCE

value is also very close to the all-time record PCE for p-i-n DMSO-free tin perovskite solar cells, which is 8.7% from our previous study[9].
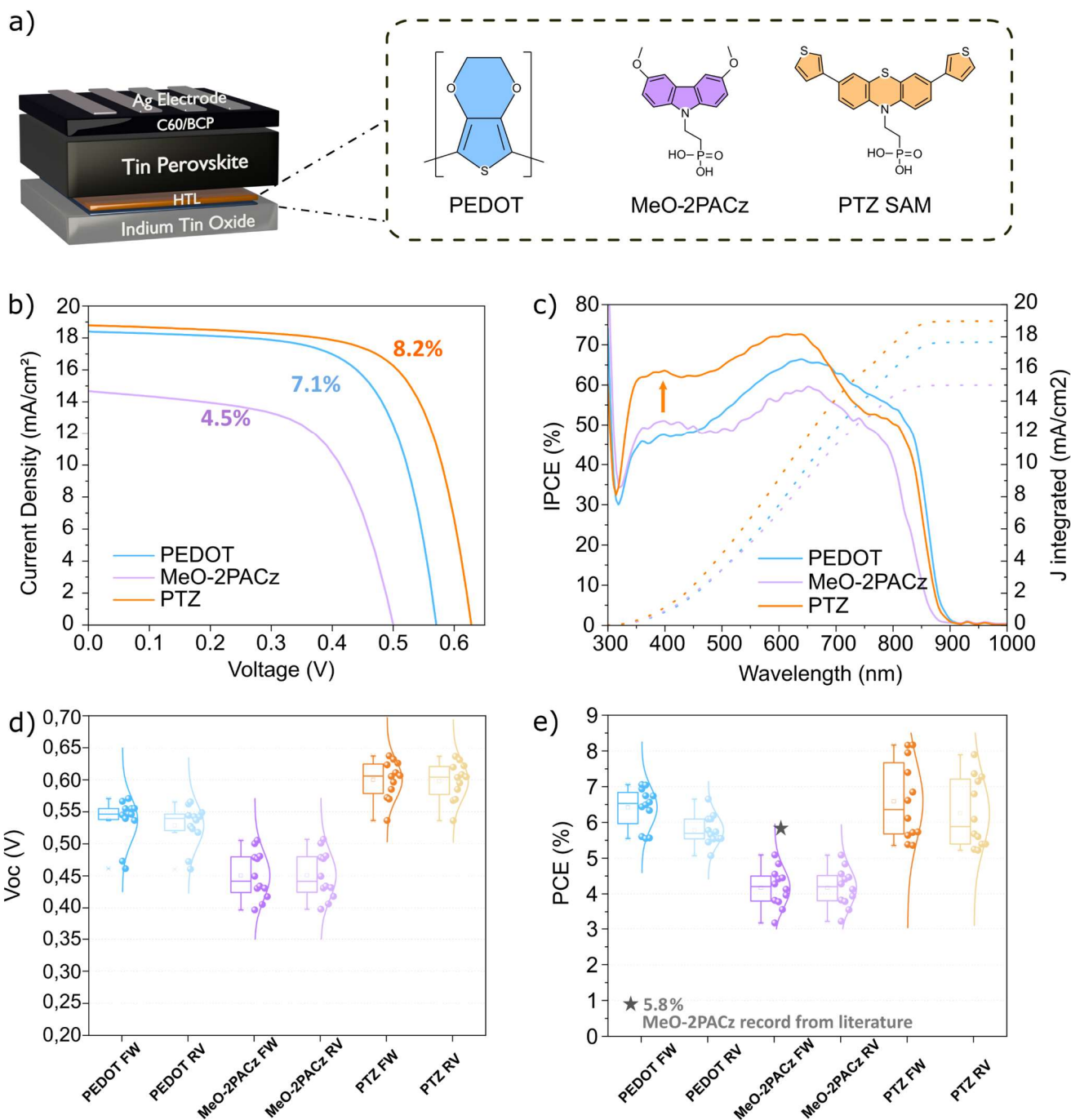
Figure 3 a) Schematic device structure of the lead-free solar cell used in this work (left) and molecular structures of the three different hole-selective materials (right). **b)** J-V characteristics and **c)** EQE spectra for the champion device for each hole-selective layer. Measured pixels in b) and c) are the same. Boxplots showing statistics for **d)** Open circuit voltage (V_{OC}) and **e)** power conversion efficiency (PCE) for the measured solar cells. In the PCE boxplots, numbers next to the normal

distribution curve indicate median values, while numbers in bold indicate champion device efficiency. Displayed with a grey star in plot e) there is the highest PCE obtained with a SAM in a DMSO-free perovskite solar cell, from the work of Aktas et al.[9]

Conclusion

In this work, we demonstrate that precise engineering of interfacial interactions is key to minimize buried interface losses and achieve efficient tin perovskite solar cells. We synthesize and characterize a new hole-selective SAM, delivering efficient p-i-n DMSO-free tin perovskite solar cells able to outperform current PEDOT devices. Density functional theory (DFT) calculations revealed that the superior performance of Th-2EPT stems from a an optimal balance between lattice compatibility and coordination strength. These insights were corroborated by multiple optical characterization techniques, such as light intensity-dependent measurements on Voc and quantum yield, ultrafast photoluminescence spectroscopy, and transient absorption spectroscopy, which all consistently demonstrated longer carrier lifetimes and reduced defect density for Th-2EPT. The improved interface quality translated into record solar cell performance, with Th-2EPT-based devices achieving a power conversion efficiency (PCE) of 8.2%, surpassing both PEDOT and MeO-2PACz. This power conversion efficiency is the highest to our knowledge for p-i-n SAM-based DMSO-free tin perovskite, and approaching the current record for DMSO-free tin perovskite.

Acknowledgments

Data Availability

The data that support the findings of this study are available from the corresponding author upon reasonable request.

References

1. Aldamasy, M. *et al*. Challenges in tin perovskite solar cells. *Phys. Chem. Chem. Phys*. **23**, 23413–23427 (2021).

2. Aktas, E. *et al*. Challenges and strategies toward long-term stability of lead-free tin-based perovskite solar cells. *Commun. Mater*. **3**, 104 (2022).

3. Abate, A. Stable Tin-Based Perovskite Solar Cells. *ACS Energy Lett*. **8**, 1896–1899 (2023).

4. Dey, K. *et al*. Substitution of lead with tin suppresses ionic transport in halide perovskite optoelectronics. *Energy Environ. Sci*. **17**, 760–769 (2024).

5. Babayigit, A. *et al*. Assessing the toxicity of Pb- and Sn-based perovskite solar cells in model organism Danio rerio. *Sci. Rep*. **6**, 18721 (2016).

6. Li, J. *et al*. Biological impact of lead from halide perovskites reveals the risk of introducing a safe threshold. *Nat. Commun*. **11**, 310 (2020).

7. Le, Z. *et al*. Ion Migration in Tin-Halide Perovskites. *ACS Energy Lett*. **9**, 1639–1644 (2024).

8. Li, G. *et al*. Ionic Liquid Stabilizing High-Efficiency Tin Halide Perovskite Solar Cells. *Adv. Energy Mater*. **11**, 2101539 (2021).

9. Aktas, E. *et al*. One-Step Solution Deposition of Tin-Perovskite onto a Self-Assembled Monolayer with a DMSO-Free Solvent System. *ACS Energy Lett*. **8**, 5170–5174 (2023).

10. Cui, D. *et al*. Making Room for Growing Oriented $FASnI_3$ with Large Grains via Cold Precursor Solution. *Adv. Funct. Mater*. **31**, 2100931 (2021).

11. Zhang, X. *et al*. The Voltage Loss in Tin Halide Perovskite Solar Cells: Origins and Perspectives. *Adv. Funct. Mater*. **32**, 2108832 (2022).

12. Xia, Y., Yan, G. & Lin, J. Review on Tailoring PEDOT:PSS Layer for Improved Device Stability of Perovskite Solar Cells. *Nanomaterials* **11**, 3119 (2021).

13. Di Girolamo, D. *et al*. Enabling water-free PEDOT as hole selective layer in lead-free tin perovskite solar cells. *Mater. Adv*. **3**, 9083–9089 (2022).

14. Cameron, J. & Skabara, P. J. The damaging effects of the acidity in PEDOT:PSS on semiconductor device performance and solutions based on non-acidic alternatives. *Mater. Horiz.* **7**, 1759–1772 (2020).

15. Kim, S. Y., Cho, S. J., Byeon, S. E., He, X. & Yoon, H. J. Self-Assembled Monolayers as Interface Engineering Nanomaterials in Perovskite Solar Cells. *Adv. Energy Mater.* **10**, 2002606 (2020).

16. Liu, M. *et al.* Compact Hole-Selective Self-Assembled Monolayers Enabled by Disassembling Micelles in Solution for Efficient Perovskite Solar Cells. *Adv. Mater.* **35**, 2304415 (2023).

17. Azam, M. *et al.* Dual functionality of charge extraction and interface passivation by self-assembled monolayers in perovskite solar cells. *Energy Environ. Sci.* **17**, 6974–7016 (2024).

18. Song, D., Narra, S., Li, M.-Y., Lin, J.-S. & Diau, E. W.-G. Interfacial Engineering with a Hole-Selective Self-Assembled Monolayer for Tin Perovskite Solar Cells via a Two-Step Fabrication. *ACS Energy Lett.* **6**, 4179–4186 (2021).

19. Fan, X. *et al.* PEDOT:PSS for Flexible and Stretchable Electronics: Modifications, Strategies, and Applications. *Adv. Sci.* **6**, 1900813 (2019).

20. Di Girolamo, D. *et al.* Enabling water-free PEDOT as hole selective layer in lead-free tin perovskite solar cells. *Mater. Adv.* **3**, 9083–9089 (2022).

21. Al-Ashouri, A. *et al.* Conformal monolayer contacts with lossless interfaces for perovskite single junction and monolithic tandem solar cells. *Energy Environ. Sci.* **12**, 3356–3369 (2019).

22. Almasabi, K. *et al.* Hole-Transporting Self-Assembled Monolayer Enables Efficient Single-Crystal Perovskite Solar Cells with Enhanced Stability. *ACS Energy Lett.* **8**, 950–956 (2023).

23. Song, D., Ramakrishnan, S., Zhang, Y. & Yu, Q. Mixed Self-Assembled Monolayers for High-Photovoltage Tin Perovskite Solar Cells. *ACS Energy Lett.* **9**, 1466–1472 (2024).

24. Liu, D. *et al.* Strain analysis and engineering in halide perovskite photovoltaics. *Nat. Mater.* **20**, 1337–1346 (2021).

25. Jiang, W., Hu, Y., Li, F., Lin, F. R. & Jen, A. K.-Y. Hole-Selective Contact with Molecularly Tailorable Reactivity for Passivating High-Performing Inverted Perovskite Solar Cells. *CCS Chem*. **6**, 1654–1661 (2024).

26. Zhang, Z. *et al*. Anchoring Charge Selective Self-Assembled Monolayers for Tin–Lead Perovskite Solar Cells. *Adv. Mater*. **36**, 2312264 (2024).

27. Liu, M. *et al*. Defect-Passivating and Stable Benzothiophene-Based Self-Assembled Monolayer for High-Performance Inverted Perovskite Solar Cells. *Adv. Energy Mater*. **14**, 2303742 (2024).

28. Love, J. C., Estroff, L. A., Kriebel, J. K., Nuzzo, R. G. & Whitesides, G. M. Self-Assembled Monolayers of Thiolates on Metals as a Form of Nanotechnology. *Chem. Rev*. **105**, 1103–1170 (2005).

29. Planells, M., Abate, A., Snaith, H. J. & Robertson, N. Oligothiophene Interlayer Effect on Photocurrent Generation for Hybrid TiO_2 /P3HT Solar Cells. *ACS Appl. Mater. Interfaces* **6**, 17226–17235 (2014).

30. Solis, O. E. *et al*. Adjusting the Crystallization of Tin Perovskites through Thiophene Additives for Improved Photovoltaic Stability. *ACS Energy Lett*. **9**, 5288–5295 (2024).

31. Pascual, J. *et al*. Lights and Shadows of DMSO as Solvent for Tin Halide Perovskites. *Chem. – Eur. J.* **28**, e202103919 (2022).

32. Al-Ashouri, A. *et al*. Monolithic perovskite/silicon tandem solar cell with >29% efficiency by enhanced hole extraction. *Science* **370**, 1300–1309 (2020).

33. Krogmeier, B., Staub, F., Grabowski, D., Rau, U. & Kirchartz, T. Quantitative analysis of the transient photoluminescence of $CH_3 NH_3 PbI_3$ /PC_{61} BM heterojunctions by numerical simulations. *Sustain. Energy Fuels* **2**, 1027–1034 (2018).

34. Treglia, A. *et al*. How Shallow and Deep Defects Drive Carrier Dynamics in Tin-Iodide Perovskites. *Adv. Energy Mater*. 2404905 (2025) doi:10.1002/aenm.202404905.

35. Saidaminov, M. I. *et al*. Conventional Solvent Oxidizes Sn(II) in Perovskite Inks. *ACS Energy Lett*. **5**, 1153–1155 (2020).

36. Alias, N. *et al*. Photoelectrical Dynamics Uplift in Perovskite Solar Cells by Atoms Thick 2D TiS$_2$ Layer Passivation of TiO$_2$ Nanograss Electron Transport Layer. *ACS Appl*. *Mater*. *Interfaces* **13**, 3051–3061 (2021).

Table of Contents

In this work, we develop Th-2EPT, a novel self-assembled monolayer (SAM), with optimized coordination strength and lattice compatibility for DMSO-free tin perovskite solar cells. Several advanced optical characterization techniques confirmed the higher quality of the Th-2EPT buried interface when compared to PEDOT and MeO-2PACz. Solar cells fabricated with Th-2EPT as the hole-selective layer achieved higher performance than PEDOT, the current state of the art hole-selective material for tin perovskite.